Design and Implementation of an Underlay Control Channel for Cognitive Radios

Daryl Leon Wasden, Hussein Moradi, and Behrouz Farhang-Boroujeny .

***Abstract*—Implementation of any cognitive radio network requires an effective control channel that can operate under various modes of activity from the primary users. This paper reports the design and implementation of a filter bank multicarrier spread spectrum (FBMC-SS) system for use as the control channel in cognitive radio networks. The proposed design is based on a filtered multitone (FMT) implementation. Carrier and timing acquisition and tracking methods as well as a blind channel estimation method are developed for the proposed control channel. We also report an implementation of the proposed FBMC-SS system on a hardware platform; a FlexRIO FPGA module from National Instruments.**

***Index Terms*—Cognitive Radio, Control Channel, Spread Spectrum Communication, Filter Banks.**

I. Introduction

CONSTRUCTION of a cognitive radio network presents a number of challenges, the most obvious of which is how to fulfill the awareness requirement. Each node must be able to sense the channel to identify the unused portions of the spectrum, and share this information with the other nodes to allow the cognitive nodes to communicate reliably while avoiding the portions of the frequency band used by legacy devices.

Various methods for channel/spectrum sensing have been explored in the literature, e.g., see [1], [2], [3]. However, the more challenging task is to find an effective method for exchanging the sensed information among the nodes within the cognitive network. Such an exchange of information clearly requires a communication channel; called control channel.

The emphasis of this paper is on the design and development of a control channel that lends itself to (i) ease of implementation, (ii) minimum interference to the primary users, and (iii) robust performance under various channel conditions. Following some logical reasoning from the present literature (see Section II), we identify spread spectrum techniques that lay a communication channel below the primary users (PUs) noise temperature, [4], as the most reasonable and reliable candidate for the control channel in cognitive radios. This is called an *underlay control channel* (UCC) for obvious reasons. We note that although direct sequence spread spectrum (DS-SS) and frequency hopping spread spectrum (FH-SS) techniques are the most widely established spread spectrum techniques, multicarrier spread spectrum (MC-SS) is a better fit for the application of interest to this paper. This follows from the fact that, compared to DS-SS and FH-SS, MC-SS is significantly more robust against narrow-band and partial-band interference, [5], [6], [7], [8], [9], and the presence of PU signals may be viewed as partial-band interference to the UCC. Moreover, as will be shown, MC-SS can be straightforwardly adapted to avoid transmission over the active PU bands. Hence, MC-SS imposes a minimum taxation to the PUs, a very desirable property.

To implement MC-SS systems two approaches are proposed in the literature. The first approach constructs an MC-SS waveform following the celebrated method of orthogonal frequency division multiplexing (OFDM), [5]. The second approach uses a filter bank multicarrier (FBMC) technique, [6], [7]. Since in the latter approach the spectrum of each subcarrier is more localized than its counterpart in the former, FBMC-based SS (namely, FBMC-SS) systems are more robust to partial-band interferences than OFDM-SS systems.

Among different choices of FBMC, we have identified filtered multitone (FMT) as the most appropriate choice for the application of interest to this paper. As demonstrated throughout this paper, FMT-SS has a number of appealing properties that lend themselves to a robust implementation. The often difficult tasks of timing and carrier synchronization can be implemented trivially, thanks to the particular properties of FMT-SS that are developed in this paper. We also propose a blind channel estimation algorithm. The estimated channel will then be used to construct a maximum ratio-combining receiver for an optimized performance, [7]. Furthermore, we report the design, implementation, and evaluation of the proposed FMT-SS scheme on a hardware platform; a National Instrument FlexRIO FPGA module.

This paper is organized as follows. In the next section, we present motivations for this work and explain why it is important in the context of cognitive radio network design. In Section III, we present an overview of the proposed FMT-SS UCC system. The details of the transmit waveform are presented in Section IV. The receiver design is discussed in detail in Section V. The theoretical designs presented in Sections IV and V are mapped to a hardware platform in Section VI. A number of novel implementation ideas have

Manuscript received 5 January 2012; revised 11 May 2012. This material is partially based upon work supported by the National Science Foundation Graduate Research Fellowship under Grant No. 0750758. This manuscript has been authored by Battelle Energy Alliance, LLC under Contract No. DE-AC07-05ID14517 with the U.S. Department of Energy. The United States Government retains and the publisher, by accepting the article for publication, acknowledges that the United States Government retains a nonexclusive, paid-up, irrevocable, world-wide license to publish or reproduce the published form of this manuscript, or allow others to do so, for United States Government purposes.

D. L. Wasden and B. Farhang-Boroujeny are with the Electrical and Computer Engineering Department at the University of Utah in Salt Lake City, Utah (e-mail: wasden@ece.utah.edu; farhang@ece.utah.edu).

H. Moradi is with Idaho National Laboratory in Idaho Falls, Idaho (e-mail: hussein.moradi@inl.gov).

Digital Object Identifier 10.1109/JSAC.2012.121104.

0733-8716/12/$31.00 © 2012 IEEE

to be introduced in this section to allow accommodation of a complete FMT-SS receiver design on the available FPGA chip (a Xilinx Virtex-5). The results of our implementation are presented in Section VII. The concluding remarks are made in Section VIII.

II. Motivation

Cognitive radios provide a promise of more efficient spectrum usage [4], [10]. Cognitive radio networks must perform several tasks to utilize the available spectrum. To avoid interfering with PUs, the nodes must perform spectrum sensing. To avoid the so-called hidden terminal problem, the spectrum usage information must be shared between nodes [11], [12], [13]. This information can either be shared locally in clustered groups [14], [15] or globally by the whole network [16], [17]. In either case, sharing spectral information requires internode communication or in other words a control channel is needed [10], [18].

In addition, many researchers focusing on medium access control (MAC) strategies for cognitive radio networks assume that a control channel is available for sharing spectral information and/or scheduling resources [19], [20], [21]. However, this by no means is a trivial task [22], and hence a variety of methods have been proposed in the literature to establish control channels for cognitive radios.

The control channels have been classified by different authors under different sub-groups, [22]. In this paper, we categorize the available control channel methods under the following sub-groups.

1) *Dedicated Control Channel (DCC):* A dedicated narrowband licensed channel is used to transmit control signals, e.g., see [23] and [24]. This method is also referred to as an out-of-band control channel, [22], because the control channel operates in a frequency band that does not overlap with any of the PU bands.
2) *Common Control Channel (CCC):* The nodes in a cognitive radio network may dynamically establish a CCC in some ad hoc manner, within the PU bands, e.g., see [14], [25], [26]. The terminology *rendezvous* is often used to refer to this type of control channel [27], [28].
3) *Underlay Control Channel (UCC):* A spread spectrum technique is adopted to establish a common control channel, e.g., see [29] and [30]. In this case, the control channel uses the entire frequency band, including portions with PU activities. However, to remain invisible to the PUs, the transmit power should be at a level comparable to the noise temperature [4].

When there is a dedicated band available for use as a DCC, then the control channel is guaranteed. This method is the simplest and when it is feasible, it is likely to be applied. However, such a dedicated channel may not always be available. For this reason, many researchers have proposed techniques of establishing a control channel either in some ad hoc manner (rendezvous or what we call a CCC) or else using a spread spectrum technique, i.e., a UCC, to mitigate the effective interference seen by PUs.

The CCC (or rendezvous) technique has been found very useful and has been well-studied [27], [28], [31], [32]. The basic idea is to send out test messages searching for the other users by hopping from one band to another until a common band is found and control messages can be sent. While this technique is very popular, there are two weaknesses. First, the hidden terminal problem when a radio cannot sense a primary transmitter, but a primary receiver is nearby thus any transmissions by this radio will result in PU interference. Second, time to rendezvous: there is always some time associated with the search for a common channel. This search must occur every time a new network is established, and it must occur every time a PU collision causes interference with an already established control channel. This problem has been addressed previously. For example in [28], a spread spectrum technique (adaptive frequency hopping) was used to avoid the need to rendezvous again in the event of a PU transmission. The use of ultra-wideband (UWB) technology to establish a control channel has also been suggested [18], [29], [33]. The interested readers may refer to [22] for a broader discussion on control channels, including various classifications.

To overcome these weaknesses, several researchers have suggested the use of spread spectrum techniques as a UCC [29], [30], [23]. This channel occupies the entire band with a low transmit power such that the PUs who are nearby will see the transmission as comparable to the noise temperature [4]. In this way, the entire band is used, but there is only a minimal impact on the PUs. The FMT-SS UCC proposed in this paper further reduces the impact of the control channel to the PUs by masking out subcarrier transmission for frequency bands that coincide with PU activities once such PU activities are recognized. This ability to dynamically select the bands of transmission may be seen as an additional bonus not offered by competing technologies, such as UWB and the traditional DS-SS and FH-SS, making the FMT-SS UCC an ideal choice for cognitive radio networks.

Multicarrier communications have been proposed for cognitive radios due to the flexibility of their spectral presence [16]. The possibility of using non-contiguous bands is noted as being particularly useful in [34]. The most prominent multicarrier technique today is OFDM. However, FBMC techniques offer many advantages over OFDM [35]. Of particular importance to cognitive radio applications is the spectral localization of the transmit power. Filter bank techniques allow the system designer to reduce the out of band leakage by increasing the order of the underlying prototype filter. In addition, filter banks can be used as both a communication method and a spectrum sensing mechanism for cognitive radios [36].

To summarize our motivations for the development of the proposed UCC, we note that it offers the following advantages:

- It does not require any dedicated band.
- Unlike CCC, there is no latency in setting up the control channel, *viz.,* the UCC is always available, irrespective of PU activities.
- Unlike DS-SS and FH-SS [27], [28], and UWB [33], [29] methods, the FMT-SS can trivially avoid the active PU bands; see Section VI-B.
- The analysis filter bank used to implement the FMT-SS receiver may also be used as a spectrum sensing mechanism [36].

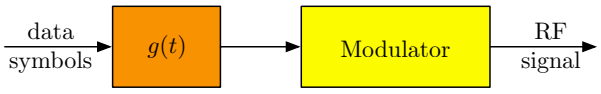

Fig. 1. Block diagram of transmitter in an FBMC-SS system.

III. Overview

Before proceeding into the details of the proposed FBMC-SS system, in this section we present a block diagram overview of the proposed transceiver. The role and significance of various sub-blocks in the system are discussed without getting ourselves involved with the mathematical details. In this way we will be able to justify our choice of FMT for FBMC-SS signaling as against other possible choices that one may think of.

In the proposed system, the transmitter is effectively a synthesis filter bank. We call this filter bank, transmitter filter bank (TxFB). The input to the TxFB is the sequence of information bits that we wish to transmit and the output of it is up-converted to a radio frequency (RF) band for transmission. As demonstrated in the next section, the TxFB is characterized by an impulse response that we represent by $g(t)$. This simplistic model of the transmitter is presented in Fig. 1.

Fig. 2 presents a block diagram of the receiver of the FMT-SS system. The receiver, after demodulating the received RF signal, passes the result through a filter matched to the transmit filter $g(t)$. As demonstrated in Section V-A, because of the special selection of the parameters in the proposed system, the output from the matched filter will be a sequence of high amplitude pulses that can be clearly identified even when the FMT-SS signal is at or below a noise level. These pulses carry the necessary information for timing and carrier acquisition as well as for their tracking. Implementation algorithms that make use of the FMT-SS signaling for timing and carrier recovery and tracking are introduced in Section VI.

The timing information and output signal from the demodulator block are passed to an analysis filter bank that extracts the received signal of the various subcarriers and samples them at the right timing phase. This information is passed to a channel estimator whose output is an estimate of the channel gain and the power of noise plus interference at each of the subcarrier bands. The last block of the receiver, called maximum ratio combining, takes the outputs of analysis filter bank and the information at the output of the channel estimator to obtain an estimate of the transmitted data symbols. The maximum ratio combining block calculates a weighted average of the detected data symbols at the output of the analysis filter bank. The less noisy outputs are given higher weights and the more noisy outputs are given lower weights.

At this point, we wish to make a few comments with regard to the choice of the FMT in our design. We note that in the context of bandwidth efficient data transmission, FMT is the least efficient method. FBMC systems that are based on cosine modulated filter banks (CMFB) and offset-QAM (OQAM) modulation allow a larger number of subcarriers per unit of bandwidth. This concept is depicted in Fig. 3.

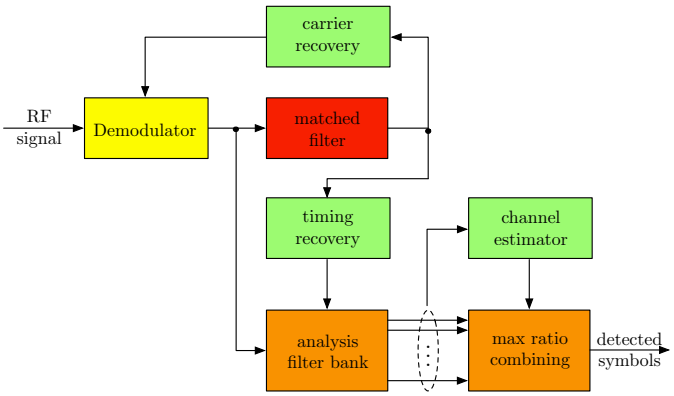

Fig. 2. Block diagram of the receiver of the proposed MC-SS system.

Clearly, if independent symbols are to be transmitted over different subcarriers, CMFB or OQAM-based FBMC will result in a higher bit rates, [35]. But, one should note that the goal here is not to increase the number of bits per unit of bandwidth. In a spread spectrum system, in general, and in the proposed FMT-SS system, in particular, the goal is to spread each information symbol over a bandwidth that is much wider than its rate, but at a level comparable or lower than the channel noise. The parameter of interest here is the *processing gain*, which is defined as the ratio of the signal-to-noise ratio (SNR) after and before the despreading at the receiver. Hence, as long as the same processing gain is established through different signaling schemes, it become immaterial to say what type of scheme is used for spreading. In an appendix, at the end of this paper, we have evaluated the processing gain of the FMT-SS and is found to be not different from an ideal FBMC-SS system with the maximum number of subcarriers in the band of transmission. It is in light of this fact that we have chosen FMT, which as will be shown throughout this paper offers simplicity in various aspects of the system implementation.

IV. Transmit Waveform

Fig. 4 presents a block diagram of the transmitter in an FBMC-SS system. Although spreading may be across a subset of subcarriers and/or may also be extended across time, in this paper we limit our design to the case where spreading is only across frequency and each data symbol is spread over all subcarriers. The input signal in Fig. 4 is a train of data symbols $s[n]$ at the spacing T. Mathematically, this is expressed as

$$s(t) = \sum_n s[n]\delta(t - nT). \tag{1}$$

Here, $h(t)$ is a common pulse-shaping filter to all subcarriers. In this paper, we refer to $h(t)$ as *prototype filter*, following the filter banks literature, [37]. Ideally, $h(t)$ should be chosen to be a well-designed lowpass filter. Accordingly, one may note that the set of filters $\gamma_0 h(t)$ through $\gamma_{N-1}h(t)$ are to band-limit the stream of data symbols and apply the spreading gain factors γ_0 through γ_{N-1}. These filters are followed by a set of modulators that shift the spectra of the band-limited signals to the set of subcarrier frequencies f_0 through f_{N-1}, hence, spread them across a broadband. We also note that Fig. 4

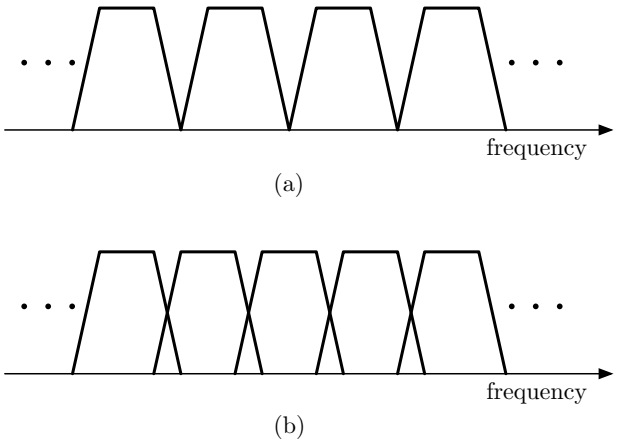

Fig. 3. Bandwidth efficiency comparison of FMT against more bandwidth efficient multicarrier schemes. (a) FMT; (b) CMFB/OQAM.

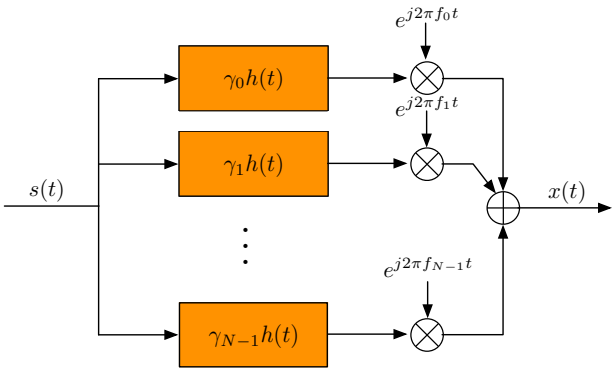

Fig. 4. Block diagram of transmitter in an MC-SS system.

is an expanded version of the first block in Fig. 1, and as demonstrated in Fig. 1, the output $x(t)$ has to be up-converted to an RF band before transmission. Here, we have ignored the modulator block for brevity. A few comments on the choice of $h(t)$ are in order. As it will become clear later, $h(t)$ should be a square-root Nyquist filter, meaning that $h(t) \star h^*(-t)$, where $\star$ denotes convolution and the superscript $*$ means conjugation, should be a Nyquist filter with regular zero-crossings at integer multiples of T. Moreover, we note that in common designs $h(t)$ is a real-valued and even function of time, i.e., $h^*(-t) = h(-t) = h(t)$. We assume this to be the case in the design that we adopt in this paper.

Using (1), the output of the transmitter is obtained as

$$x(t) = \sum_n \sum_{k=0}^{N-1} \gamma_k s[n] h(t - nT) e^{j2\pi f_k t}. \tag{2}$$

When the subcarrier frequencies f_k are selected such that $f_k T$, for $k = 0, 1, \cdots, N-1$, is an integer, $e^{j2\pi f_k t} = e^{j2\pi f_k (t-nT)}$. We assume this is the case in our design. Hence, (2) can be rearranged as

$$x(t) = \sum_n s[n] g(t - nT) \tag{3}$$

where

$$g(t) = h(t) p(t) \tag{4}$$

and

$$p(t) = \sum_{k=0}^{N-1} \gamma_k e^{j2\pi f_k t}. \tag{5}$$

Note that $g(t)$ is factored as a multiplication of the prototype filter $h(t)$ and another function of time, $p(t)$, that is determined by the spreading gains γ_k and the subcarrier frequencies f_k.

Equation (3) has the following interpretation. The MC-SS signal $x(t)$ is obtained by passing the data stream $s[n]$ through the pulse shaping filter $g(t)$. The choice of $g(t)$, determined by $h(t)$, γ_ks, and f_ks, can result in various forms of MC-SS systems. When $h(t)$ is a rectangular pulse with a width of T equal to the length of FFT (in an OFDM system), $T_{\rm FFT}$, plus the length of a cyclic prefix, $T_{\rm CP}$, and f_k are at the regular interval $1/T_{\rm FFT}$, $x(t)$ will be an OFDM-based SS signal, hence, may be referred to as OFDM-SS. On the other hand, if $h(t)$ is the impulse response of a square-root raised-cosine filter with a roll-off factor α and a symbol rate $1/T$, and the frequencies f_k are at a regular interval $(1+\alpha)/T$, $x(t)$ will be an FMT-based spread spectrum signal, i.e., the FMT-SS design that we develop in this paper. Other choices of $h(t)$ and f_k that lead to other types of FBMC-SS are also possible (e.g., CMFB and OQAM-based systems); see [38] for a review of various forms of FBMC systems.

The emphasis of this paper is on the design and implementation of an FMT-SS system. As noted earlier, the choice of FMT for multicarrier modulation is to take advantage of its simplicity which, in turn, results in a simple and robust FBMC-SS system. In our design, we assume that N is even, set $\alpha = 1$, and spread the subcarrier frequencies f_k at the positions $\pm\frac{1}{T}$, $\pm\frac{3}{T}$, $\cdots$, $\pm\frac{N-1}{T}$. More specifically, we let $f_0 = -\frac{N-1}{T}$, $f_1 = -\frac{N-3}{T}$, $\cdots$, $f_{N-1} = \frac{N-1}{T}$. The spreading gain factors γ_k are chosen as

$$\gamma_k = e^{j\theta_k}, \quad \text{for } k = 0, 1, \cdots, N-1. \tag{6}$$

where the angles θ_k are a set of phase angles that may be chosen to improve on the properties of the FMT-SS waveform. Among various choices, $\theta_k = \pi k^2/N$ is an interesting one. It belongs to the class of polyphase codes [39]. It leads to a transmit signal $x(t)$ with a moderately low peak-to-average-power ratio (PAPR); a consideration that one may wish to take note of in designing the pulse-shape $g(t)$. In any case, for our later reference, we note that for all choices of θ_k, according to (6), the following identities always hold:

$$|\gamma_k|^2 = 1, \quad \text{for } k = 0, 1, \cdots, N-1. \tag{7}$$

Although the formulations given above are in terms of continuous time signals and filters, practical generation of the transmit waveform is conveniently performed in discrete time using efficient signal processing blocks. More specifically, the transmit waveform is generated using the structure presented in Fig. 5, where $\uparrow L$ denotes an L-fold expander and $g[n]$ is the corresponding discrete-time version of $g(t)$. Moreover, the system presented in Fig. 5 can be most efficiently implemented according to a polyphase structure; e.g., see [37], [40] for details.

Fig. 5. Digital implementation of transmitter in an MC-SS system.

V. Receiver Design

In this section, we discuss the mathematical basis for the implementation of the various blocks in the receiver structure that was introduced earlier in Fig. 2. The transfer of the developed/proposed mathematical formulations to an FPGA implementation is discussed in Section VI.

A. Preliminaries

Clearly, any carrier and timing recovery method should take advantage of the properties of the modulation method that has been used to construct the transmitted signal. We thus begin our discussion here by exploring some of the properties of the pulse-shape $g(t)$.

Consider the case where the channel is ideal and demodulation is performed perfectly, hence, the demodulator output is the transmit baseband signal $x(t)$ given by (3). Passing this through a filter matched to the transmit pulse shape $g(t)$, the overall impulse response of the system is obtained as

$$\eta(t) = g(t) \star g^*(-t). \tag{8}$$

Using (4) and (5) in (8) and noting that by design $h(-t) = h(t)$, we obtain

$$\eta(t) = \left(\sum_{k=0}^{N-1} \gamma_k h(t) e^{j2\pi f_k t} \right) \star \left(\sum_{l=0}^{N-1} \gamma_l^* h(t) e^{j2\pi f_l t} \right). \tag{9}$$

Next, we note that, $h(t)e^{j2\pi f_k t}$ and $h(t)e^{j2\pi f_l t}$ may be thought as a pair of filters. By design, such a pair of filters either have a common band (when $f_k = f_l$) or cover non-overlapping bands. In the latter case, $h(t)e^{j2\pi f_k t} \star h(t)e^{j2\pi f_l t} = 0$. Hence, (9) reduces to

$$\eta(t) = \sum_{k=0}^{N-1} |\gamma_k|^2 \left(h(t)e^{j2\pi f_k t} \star h(t)e^{j2\pi f_k t} \right). \tag{10}$$

Straightforward manipulations of (10) and recalling (7), lead to

$$\eta(t) = \beta(t)\rho(t) \tag{11}$$

where $\rho(t) = h(t) \star h(t)$, by design, is a Nyquist pulse whose peak appears at $t = 0$, and

$$\beta(t) = \sum_{k=0}^{N-1} e^{j2\pi f_k t}. \tag{12}$$

One may notice that $\beta(t)$ is the summation of N complex sine-waves all of the amplitude unity. Hence, the Fourier transform of $\beta(t)$ is effectively a sampled version of a rectangular pulse, as demonstrated in Fig. 6. Note that the samples in the frequency domain are spaced by $2/T$. This implies that $\beta(t)$ is a train of sinc pulses spaced in time at the interval $T/2$. At $t = 0$ and non-integer multiples of T, all the components of $\beta(t)$ have zero phase and, thus, add up to the value N. At the points where t is an odd multiple of $T/2$, all the components of $\beta(t)$ have phase of π, thus, add up to the value of $-N$. An example of $\beta(t)$ for the case where $N = 16$ is presented in Fig. 7. As N increases and approaches infinity, the sinc train approaches an impulse train and, thus, $\eta(t)$ will approach a waveform consisting of a number of impulses (narrow and tall pulses, when N is finite, but large) whose magnitudes are the samples (or the negated samples) of the Nyquist pulse $\rho(t)$. Interestingly, when the roll-off factor $\alpha = 1$, one finds that there are only three non-zero samples of $\rho(t)$, with values of -0.5, 1, and -0.5 at the positions $t = -T/2$, 0, and $T/2$, respectively. Hence, when $\alpha = 1$ and $N \to \infty$,

$$\eta(t) = -0.5\delta(t + T/2) + \delta(t) - 0.5\delta(t - T/2). \tag{13}$$

This result becomes an approximation when N is finite, but sufficiently large. A more precise expression will be to define

$$\beta_0(t) = \beta(t)\Pi\left(\frac{t}{T_0}\right) \tag{14}$$

where $\Pi(\frac{t}{T_0})$ denotes a rectangular pulse with a properly chosen width of T_0 and, accordingly, write (13) as

$$\eta(t) = -0.5\beta_0(t + T/2) + \beta_0(t) - 0.5\beta_0(t - T/2). \tag{15}$$

Equation (15) is the system response between the input $s(t)$ and the output of the matched filter $g^*(-t)$. Hence, using (1),

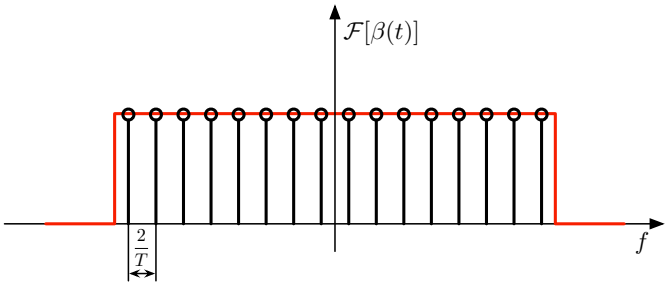

Fig. 6. Demonstration of the Fourier transform of $\beta(t)$.

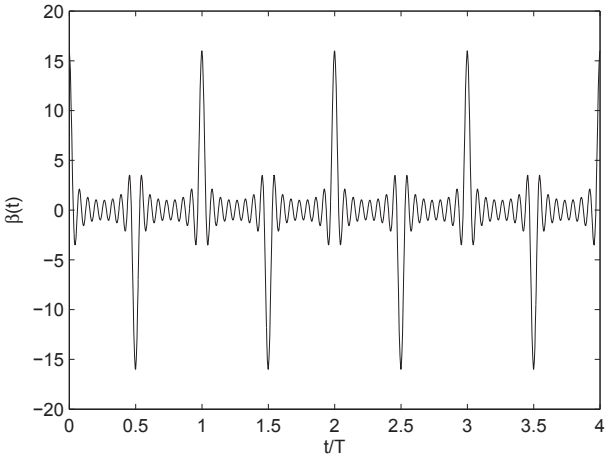

Fig. 7. An example of $\beta(t)$.

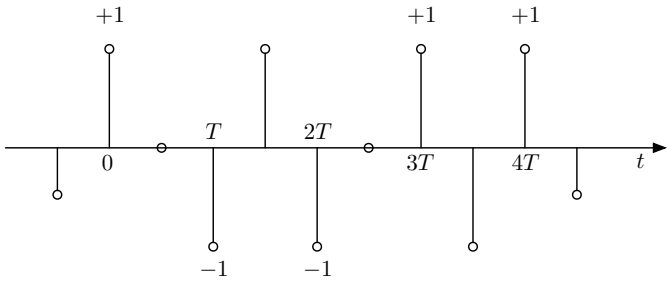

Fig. 8. A typical signal exemplifying $z(t)$. In this example, the transmitted symbol sequence is $s[n] = \{+1, -1, -1, +1, +1\}$.

one finds that the output of the matched filter is given by

$$z(t)=\sum_n s[n]\left(-0.5\beta_0\left(t+\frac{T}{2}-nT\right)+\beta_0(t-nT) -0.5\beta_0\left(t-\frac{T}{2}-T\right)\right)+\nu_0(t). \quad (16)$$

Fig. 8 presents a typical signal at the matched filter output, where, for clarity of presentation, $\beta_0(t)$ is replaced by a unit impulse. Note that at the position nT, an impulse with amplitude $s[n]$ appears. At mid-point $(n+0.5)T$, $z(t)$ is zero, if $s[n] \neq s[n+1]$, or is an impulse with amplitude $-s[n]$, if $s[n] = s[n+1]$.

Next, we discuss the effects of non-idealities in the channel.

1) Impact of carrier frequency offset: Assuming that the channel is ideal, but there exists a carrier frequency offset Δf_c between the transmitter and receiver, (9) will become

$$\eta(t) = \left(\sum_{k=0}^{N-1}\gamma_k h(t)e^{j2\pi(f_k+\Delta f_c)t}\right)\star\left(\sum_{l=0}^{N-1}\gamma_l^* h(t)e^{j2\pi f_l t}\right). \quad (17)$$

For the case where $0 < \Delta f_c < 2/T$, subcarrier filters at bands k and $k+1$ will overlap with the transmitted signal from the kth band. Noting this, from (17), we obtain

$$\eta(t)=\sum_{k=0}^{N-1}\left(h(t)e^{j2\pi(f_k+\Delta f_c)t}\star h(t)e^{j2\pi f_k t}\right) +\sum_{k=0}^{N-2}\gamma_k\gamma_{k+1}^*\left(h(t)e^{j2\pi(f_k+\Delta f_c)t} \star h(t)e^{j2\pi(f_k+\frac{2}{T})t}\right). \quad (18)$$

Straightforward manipulation of the terms in (18) leads to

$$\eta(t)=\beta(t)\left(h(t)e^{j2\pi\Delta f_c t}\star h(t)\right) +\kappa(t)\left(h(t)e^{j2\pi(\Delta f_c-\frac{2}{T})t}\star h(t)\right) \quad (19)$$

where $\beta(t)$ is given by (12) and

$$\kappa(t) = e^{j(4\pi/T)t}(\beta(t) - e^{j2\pi f_0 t}). \quad (20)$$

To simplify (19), we note that for typical values of N, the term $e^{j2\pi f_0 t}$ in (20), compared to $\beta(t)$, is negligible, and thus may be ignored. In addition, $\beta(t)$ is significant for values of t in the vicinities of multiples of $T/2$, and for these choices of t, $e^{j(4\pi/T)t} \approx 1$. Considering these approximations, (19) may be replaced by

$$\eta(t) = \beta(t)\varrho(t) \quad (21)$$

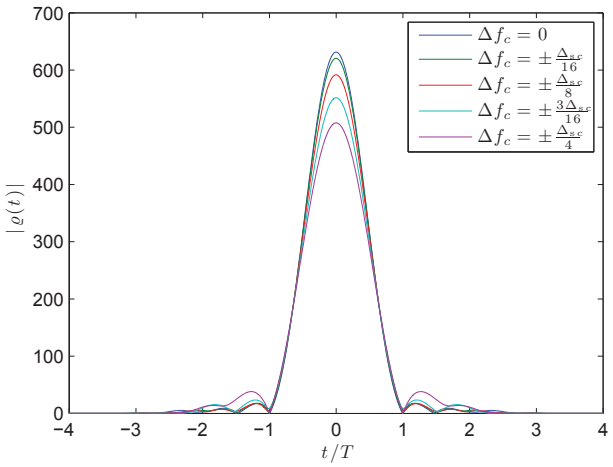

Fig. 9. Plots of $|\varrho(t)|$ for different choices of Δf_c. $\Delta_{\rm sc} = 2/T$ denotes the spacing between subcarriers.

where

$$\varrho(t) = h(t)e^{j2\pi\Delta f_c t}\star h(t) + h(t)e^{j2\pi(\Delta f_c-\frac{2}{T})t}\star h(t). \quad (22)$$

Clearly, for $\Delta f_c = 0$, $\varrho(t)$ reduces to $\rho(t)$. As Δf_c deviates from zero, $\varrho(t)$ deviates from $\rho(t)$. However, some special features of it that can be used for synchronization purposes still remain nearly the same. In particular, $|\varrho(t)|$ preserves the shape of $|\rho(t)|$ to a great extent and its amplitude reduces only slightly over a relatively wide range of Δf_c. To demonstrate this, a set of plots of $|\varrho(t)|$ for different choices of Δf_c are presented in Fig. 9.

2) Impact of the channel impulse response: When the channel is non-ideal, i.e., $c(t) \neq \delta(t)$, $\eta(t)$ of (13) becomes

$$\eta(t) = -0.5c'(t+T/2) + c'(t) - 0.5c'(t-T/2) \quad (23)$$

where

$$c'(t) = c(t)\star\beta_0(t). \quad (24)$$

For sufficiently large values of T, the three terms on the right-hand side of (23) remain non-overlapping. In fact, for typical values of T and the spread of channel impulse response, $c'(t)$ always remain a relatively narrow and tall pulse, or a cluster of narrow and tall pulses; see Fig. 16, below, for measurement results. In Section VI, we use the above results to suggest methods for timing recovery and carrier synchronization.

B. Timing recovery

As discussed above, the matched filter output $z(t)$ consists of a sequence of narrow pulses at the spacing of $T/2$. These pulses are always present at the time instants that are even multiples of $T/2$ and these correspond to the center of the data symbols. On the other hand, at the time instants that are odd multiples of $T/2$, the presence of such pulses depends on the information symbols transmitted before and after the time instant. As demonstrated in Fig. 8, a pulse will appear only when the two symbols are the same.

Obviously, many methods exist for using the properties of these pulses to find the time instants associated with the even factors of $T/2$ – the desired time instants. One particular

choice of these methods that provides a good match to the hardware setup discussed in Section VI-A is presented in Section VI-E.

C. Carrier recovery

Algorithms for carrier acquisition and tracking can also be devised by taking advantages of the pulses generated at the output of the matched filter. Such algorithms are developed in Section VI.

D. Channel estimation

Once the received signal is carrier compensated and the timing information is obtained, the sampled signal at the outputs of the receiver analysis filter bank satisfies the following set of equations:

$$z_k(nT) = \gamma_k C_{\mathrm{BB}}(e^{j2\pi f_k}) s[n] + \vartheta_k(nT), \quad \text{for } k = 0, 1, \cdots, N-1 \tag{25}$$

where $C_{\mathrm{BB}}(e^{j2\pi f_k})$ is the equivalent baseband channel frequency response at the frequency f_k and $\vartheta_k(nT)$ arises from the contributions from noise and interfering signals that may exist in the band of transmission. We assume the channel impulse response contains M samples, and using this a priori information we perform a standard least squares estimator to obtain the frequency response of the channel $\hat{C}_{\mathrm{BB}}(e^{j2\pi f_k})$.

When $s[n]$ is known, this technique provides a unique estimate. When $s[n]$ is unknown, it provides an estimate with a sign ambiguity, since $s[n] = \pm 1$.

As discussed in the next section, the implementation of an optimum receiver, through maximum ratio combining, requires the estimates of the variance of each element of the interference vector $\boldsymbol{\vartheta}(nT)$. Once the channel estimate is obtained, these interference/noise estimates can be easily calculated by averaging the magnitude squared of

$$\vartheta_k(nT) = z_k(nT) - s[n]\gamma_k \hat{C}_{\mathrm{BB}}(f_k) \tag{26}$$

over a few choices of n.

E. Maximum ratio combining

Following the principle of maximum ratio combining, [41], an unbiased minimum variance estimate of $s[n]$ is obtained as

$$\hat{s}[n] = \mathbf{w}_o^{\mathrm{H}} \mathbf{z}(nT), \tag{27}$$

where $\mathbf{z}(nT) = \left[\ z_0(nT) z_1(nT) \cdots z_{N-1}(nT)\ \right]^{\mathrm{T}}$ and the tap-weight vector $\mathbf{w}_o$ is given by

$$\mathbf{w}_o = \frac{1}{\sum_{k=0}^{N-1} \frac{|\hat{C}_{\mathrm{BB}}(e^{j2\pi f_k})|^2}{\sigma_k^2}} \begin{bmatrix} \frac{\gamma_0 \hat{C}_{\mathrm{BB}}(e^{j2\pi f_0})}{\sigma_0^2} \\ \frac{\gamma_1 \hat{C}_{\mathrm{BB}}(e^{j2\pi f_1})}{\sigma_1^2} \\ \vdots \\ \frac{\gamma_{N-1} \hat{C}_{\mathrm{BB}}(e^{j2\pi f_{N-1}})}{\sigma_{N-1}^2} \end{bmatrix}. \tag{28}$$

Here, σ_k^2 is the variance of $\vartheta_k(nT)$ which is obtained by averaging the magnitude squared output of (26).

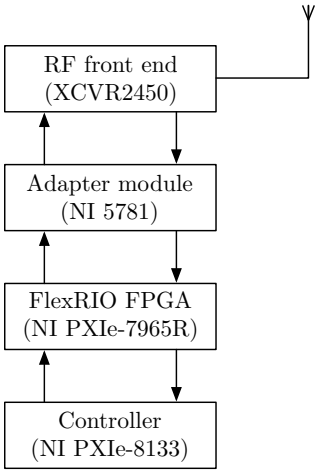

Fig. 10. A block diagram symbolizing data flow of the hardware setup used for implementation.

VI. System Implementation

A. System setup

The platform chosen for development of a prototype system is a National Instruments (NI) FlexRIO FPGA module combined with an NI FlexRIO adapter module, an NI real-time controller, and an Ettus RF front end (daughter board only). The FlexRIO module is an NI PXIe-7965R. This module is equipped with a Xilinx Virtex-5 FPGA and 512 MB of onboard memory (DRAM). The NI FlexRIO adapter module is an NI 5781. This module is equipped with dual 100 MS/s 14-bit analog-to-digital converters (for the receive side) and dual 100 MS/s 16-bit digital-to-analog converters (for the transmit side). The NI Real-Time Controller is an NI PXIe-8133. This controller basically is a host PC. It is equipped with an Intel Core i7-820 processor (1.73 GHz quad-core) and 4 GB of RAM. The controller is running a real-time operating system which is programmable using NI LabVIEW Real-Time. Communication between the controller and the FPGA module is facilitated by a high speed Direct Memory Access (DMA) interface. The Ettus RF front end is an XCVR2450 operating in the 2.4 to 2.5 GHz band.

This system was chosen for its flexibility and programmability. The interconnections between different modules (similar for both the transmitter and receiver) are presented in Fig. 10. While most of the signal processing is implemented on the FPGA module, the structurally more complicated and less time critical components of the system (namely, channel estimation and computation of MRC coefficients) are delegated to the controller. These are updated in real-time, but are required less often compared to the timing and carrier recovery portions of the system.

To allow convenient filtering of the out-of-band signal images after DAC, at the transmitter, the synthesized signals are generated at double the minimum required rate. Similarly, at the receiver, the demodulated baseband signal is sampled at twice its Nyquist rate. The N subcarriers are spread over a bandwidth of 25 MHz. This translates to a symbol rate

$$\frac{1}{T} = \frac{25}{2N} = \frac{12.5}{N} \text{ MHz}.$$

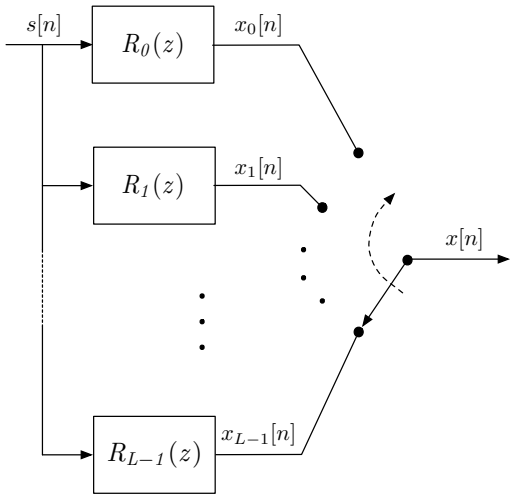

Fig. 11. A polyphase implementation of the transmitter structure of Fig. 5.

For $N = 500$, as an example, this results in a bit rate of 25 kb/s for the UCC, if, as assumed in the previous sections of this paper, $s[n]$ is chosen from a BPSK alphabet.

B. Transmitter implementation

The transmitter is a relatively small part of the overall transceiver design, but a few considerations will lead to a better system implementation. Two possibilities exist for the transmitter implementation: (i) When the spreading gains γ_k are fixed, one may choose to implement the structure presented in Fig. 5, following a basic polyphase structure, [37]. (ii) To mitigate interference with PUs, subcarriers corresponding to the detected PU activity may be masked out if a polyphase synthesis filter bank is chosen as shown in Fig. 4. As discussed below, the first method results in an implementation with very low complexity, while the second approach provides more flexibility.

Fig. 11 presents a polyphase implementation of the transmitter structure of Fig. 5, i.e., an implementation based on the first method. An interested reader should see [37] for detailed derivation of this structure. In Fig. 11, $R_0(z)$ through $R_{L-1}(z)$ are Type 2 polyphase components of $G(z)$, where $G(z)$ is the z-transform of $g[n]$. We note that each polyphase component has only a small number of coefficients, equal to the length of $g[n]$ divided by L. Moreover, since $s[n]$ takes only values of $+1$ and -1, computation of each output sample of Fig. 11 requires only a few add/subtract operations.

Fig. 12 presents a polyphase implementation of the transmitter structure according to the second method. This structure is, of course, significantly more complex than the first method. However, it provides flexibility that proves very useful in cognitive radio applications. To eliminate the UCC's interference to the PUs (consistent with the goals of cognitive radios), the subcarriers that coincide with detected PU activity may be masked out in a dynamic fashion. Thus, all interference with PUs is eliminated as soon as the transmitter recognizes the presence of PUs through its chosen spectrum sensing mechanism.

Clearly, the choice between either of the two methods is that of the designer. One can choose the first method, if the complexity is the main criterion. On the other hand, the second method may be chosen, if the flexibilities that it offers are critical to the design. We have implemented both methods in our system.

C. Receiver implementation

Typically, the receiver in a communication system is more complicated than its transmitter counterpart. In the receiver, efforts have to be made to recover and compensate for timing error, carrier offset, and channel effects (fading, noise, etc).

The receiver implementation presented here uses a simple finite state machine to control a sequence of events, following the structure presented in Fig. 2. Once the receiver is turned on, the state machine executes the following steps in order:

1) By sliding the timing phase at the input to the matched filter, the matched filter output is examined to find the large peaks. As discussed in the previous sections, large peaks will be seen at the desired timing phase or at the points that are offset by $T/2$. Therefore, this step finds the timing phase with an ambiguity of $T/2$ seconds. Once this step is complete, the following two steps, that are run simultaneously, will search for any carrier offset and resolve the timing ambiguity $T/2$.
2) The carrier acquisition is performed by considering the property of the matched filter output signal which is presented in Fig. 8. More details are given in Section VI-F.
3) The ambiguity of the $T/2$ timing phase is resolved by comparing the signal powers at odd and even multiples of $T/2$. The one with the higher power will be the correct timing phase.
4) Once the correct timing phase and carrier are acquired, the state machine enters a tracking mode where the timing phase and carrier frequency are further tuned and tracked. The details of these are given below.
5) While the system is in tracking mode, the channel estimation is performed and subsequently the MRC and data detection are made.

These events must occur in the proper sequence for the receiver to be synchronized to the transmitter for a viable communication. For the optimal detector that we are proposing in this paper, the receiver must use an analysis filter bank. For this reason, we propose to calculate the matched filter output based on the filter bank outputs. This choice has several benefits that occur during the synchronization sequence. Fig. 13 presents a block diagram of the receiver that follows this philosophy. The polyphase analysis filter bank is common to the subsequent blocks; namely, channel estimator, maximum ratio combiner (MRC), and matched filter output calculator. The latter feeds the carrier and timing recovery loop filters. Next, we expand on the details of these blocks.

D. Matched Filter Output Calculator

The outputs of the analysis filter bank can be used to calculate the outputs of the matched filter by first despreading them (i.e., multiplying by the conjugate of the spreading gains)

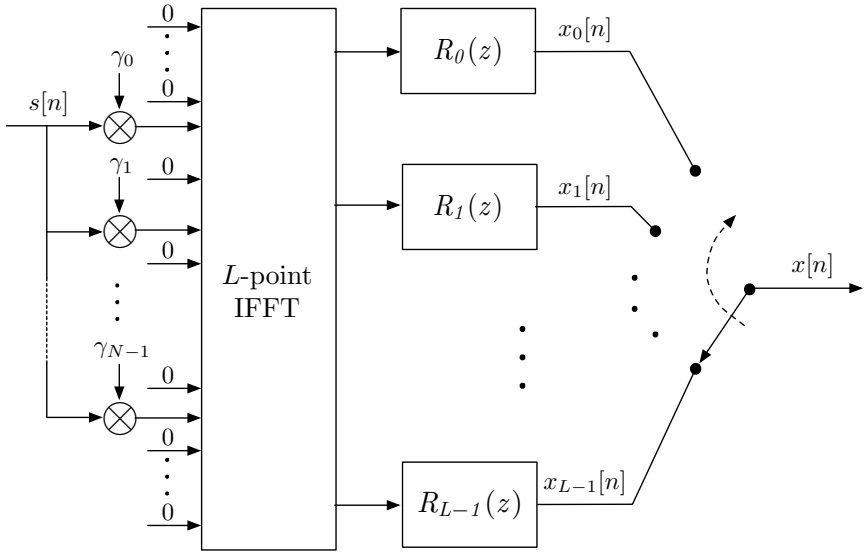

Fig. 12. Block diagram of a synthesis filter bank implementation at the transmitter, according to the second method. The zero inputs to the IFFT at the top and bottom are to insert guard bands at the two sides of the baseband signal. It simplifies filtering after DAC. Additional zeros inserted after each active subcarrier, as per discussion in Section IV.

and, then, adding the results. The matched filter output thus is given by

$$z(nT/2) = \sum_{k \in \mathcal{K}} \gamma_k^* z_k(nT/2) \tag{29}$$

where $z_k(nT/2)$ are the output samples from the analysis filter bank.

For the purpose of timing phase tracking, we require samples of the matched filter output slightly before and slightly after the present time, say, $nT/2 + \Delta t$ and $nT/2 - \Delta t$, where Δt is some small delay. To this end, we note that each channel output in the filter bank is a narrowband signal. When a sufficiently narrowband signal passes through a delay, $\pm\Delta t$, the delay may be approximated as a complex gain $e^{\pm 2\pi f_k \Delta t}$ at the kth subcarrier band. Hence, to calculate the matched filter output at $nT/2 + \Delta t$ and $nT/2 - \Delta t$, in addition to the one at $nT/2$, we include the gains $e^{\pm 2\pi f_k \Delta t}$ into the spreading gains γ_k^* in formulae similar to (29). These along with the result from (29) provide three samples of the matched filter output every $T/2$ seconds that are either all or partially used for the procedures listed in the following subsections.

E. Timing Acquisition

The timing acquisition is broken into two parts during Steps 1 and 3 of the state machine progression. Step 1 requires a sample slider. This is a device which allows a shift in the timing phase by one sample in either a positive or negative direction. Many options are open to a designer for implementation of the sample slider. We choose a design that is convenient for our polyphase filter bank implementation.

The sample slider can be represented by a variable delay z^{-D} where D is an integer such that $0 \leq DT_s < T/2$, where T is the symbol period and T_s is the sampling interval. L represents the total number of subcarriers in the system and is equal to the integer value T/T_s. In terms of L, $0 \leq D < L/2$. Obviously, we may equivalently consider this delay as part of our input sequence or as part of our prototype filter.

For the polyphase filter bank implementation, the prototype filter $h[n]$ is divided into its L polyphase components, say, $E_0(z)$ through $E_{L-1}(z)$. Let

$$H(z) = \sum_{n=0}^{KL-1} h[n] z^{-n}. \tag{30}$$

The kth polyphase component of $H(z)$ is thus given by

$$E_k(z) = \sum_{l=0}^{K-1} h[k + lL] z^{-l}. \tag{31}$$

Note that the length of $h[n]$ is assumed to be KL, hence, each polyphase component has K coefficients.

If we wish to include the sample slider (a variable delay) in the prototype filter, then the new prototype filter $f[n]$ is actually equal to a shifted version of the old prototype filter, i.e., $f[n] = h[n - D]$. This implies that $F(z) = z^{-D} H(z)$ whose kth polyphase component is obtained as

$$E'_k(z) = \sum_l h[k + lL - D] z^{-l} \tag{32}$$

where it is understood that $h[n]$ is zero outside of the range $0 \leq n < KL$. Careful examination of (32) and its comparison with (31) reveal that

$$E'_k(z) = \begin{cases} z^{-1} E_{L+k-D}(z) & k < D \\ E_{k-D}(z) & k \geq D. \end{cases} \tag{33}$$

Therefore, we recognize that we can implement the slider by circularly shifting the polyphase components and adding a unit delay for $k < D$. This sample delay also creates an additional artificial delay in the channel impulse response which leads to a linear phase offset on each subcarrier. Circularly shifting the subcarrier inputs to the FFT can compensate for this additional

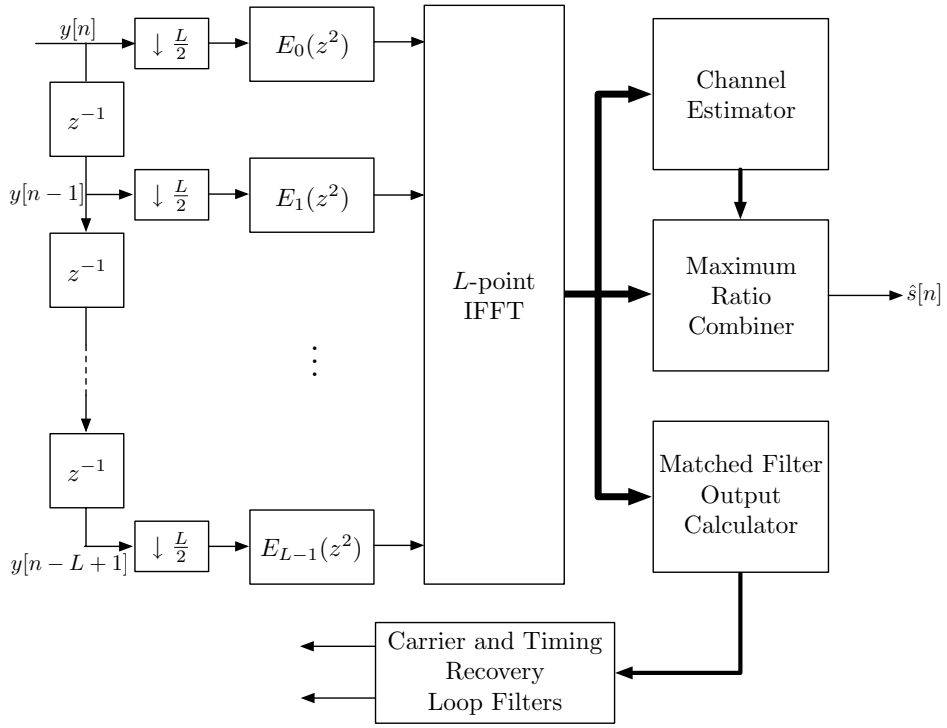

Fig. 13. Block diagram of the polyphase analysis filter bank used in the receiver design.

delay without requiring an update to the channel estimates on each subcarrier.

In Step 1 of the synchronization sequence, the input timing phase is varied through its entire range, from $D = 0$ to $D = L/2 - 1$. The output power is averaged over several samples, and the maximum average power is recorded. Subsequently, D is fixed to this value.

Following this, during Step 3 of the synchronization sequence, the average output power of the even and odd samples $z(nT)$ and $z(nT + T/2)$, respectively, of the matched filter output are computed. Whichever set of samples results in a higher average power is selected as the correct timing phase. These samples are fed to the channel estimator and MRC blocks.

F. Carrier Acquisition

Initial carrier acquisition occurs during Step 2 of the synchronization sequence. From the example presented in Fig. 8, one will note that, in the absence of the channel noise and in the presence of a carrier offset Δf_c, for any arbitrary n,

$$\begin{aligned}\zeta(n) &= z^*(nT/2)z((n+1)T/2) \\ &= \begin{cases} -ae^{j2\pi\Delta f_c T/2} & \text{adj. symbols identical} \\ 0 & \text{adj. symbols differ} \end{cases} \end{aligned} \tag{34}$$

where a is some positive constant that depends on the signal level. In other words, the frequency offset can be extracted from $\zeta(n)$when the underlying adjacent symbols are identical. When the underlying adjacent symbols differ, the magnitude of $\zeta(n)$ is zero. The presence of channel noise results in samples of $\zeta(n)$ that will be noisy. Hence, one may find that an estimate of Δf_c can be obtained as

$$\Delta f_c = \frac{1}{\pi T}\angle\{-\text{avg}[\zeta(n)]\}. \tag{35}$$

G. Tracking

Once the carrier offset and timing phase have been acquired, a small residual error may remain due to noise. Also, slight drifts in the oscillators used at the transmitter and receiver may result in small errors accumulating as time progresses. To overcome both of these challenges, tracking mechanisms must be put in place.

For carrier tracking, we may use the same observations made for carrier acquisition. As such, we propose the following update equation:

$$\Delta f_c(n) = \Delta f_c(n-1) + \frac{\mu}{\pi T}|\zeta(n)|\angle\{-\zeta(n)\}. \tag{36}$$

In (36), μ is a step-size parameter used to control the impact of noise on the system. The addition of $|\zeta(n)|$ in the update term is to make sure that when $\zeta(n)$ is small and hence will be significantly affected by noise, the associated update will be (effectively) discarded. We note that (36) is a first order phase locked loop (PLL). Clearly, higher order PLLs can be also implemented.

For timing phase tracking, we use the difference between the two offset outputs from the matched filter. If the system is already locked near the correct timing phase, then the difference is an error signal which can be used to adaptively update a phase offset. The reader can verify this by examining the peak shown in Figure 9. This is a variant of the well-known early/late gate technique [40]. An operation similar to despreading can be used to calculate this error as shown here.

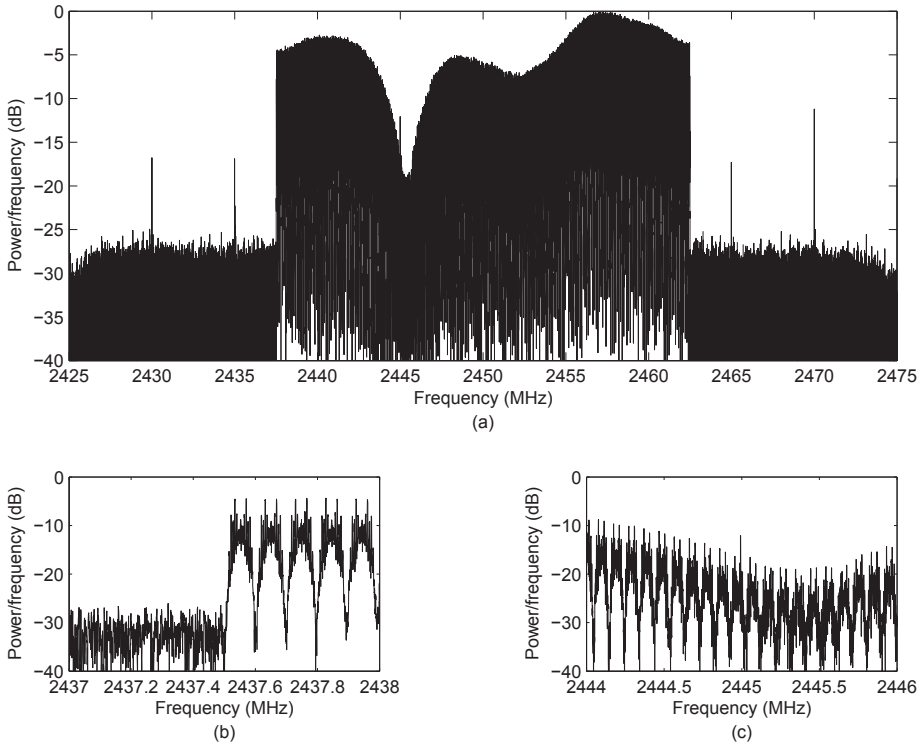

Fig. 14. A snap-shot of the measured power spectral density of the received FMT-SS signal. (a) The overall spectrum. (b) The spectrum at the beginning of the frequency band. (c) The spectrum around the null of the spectrum.

$$e_D[n] = |z[nT/2 + \Delta t]|^2 - |z[nT/2 - \Delta t]|^2 \qquad (37)$$

The update equation uses this error and follows the intuition: simply move in the direction of increasing amplitude along the envelope $\varrho(t)$. Following an update to $e_D[n]$, the variable delay $D[n]$ is updated as

$$D[n] = D[n-1] + \mu e_D[n]. \qquad (38)$$

To reduce the effects of noise, a step-size parameter μ has been included. Note that only the integer part of D is used when choosing the timing offset for the sample slider.

H. Channel Estimation and Maximum Ratio Combiner

The channel estimation and computation of MRC coefficients are the most complex part of the receiver. However, fortunately, these calculations are not time critical and thus can be implemented on the controller. Moreover, to make sure that the results do not suffer from any serious round-off noise problem, the implementation will be in floating point (as against the rest of the system which is implemented in fixed point on the FPGA). The computed MRC coefficients are periodically transferred to the FPGA module for real-time computation of the MRC output.

VII. Results of Implementation

The UCC proposed and developed in the previous sections need to be deployed in an actual cognitive radio network to prove its effectiveness. Such deployment is currently under study and its results will be reported in future publications. In this section, we present some results from the developed system to confirm the theoretical results of Sections IV and V.

To highlight the main features of FMT-SS signals, we begin with a study of an example of a relatively strong transmit signal, such that its details can be observed at the receiver. However, we note that in a practical cognitive radio one wishes to keep the received signal at a level comparable to or below the noise floor. For our later experiments, we will reduce the signal level to a level comparable to noise. The signal is an FMT-SS signal with a total of $N = 256$ active subcarriers. The transmission is over a bandwidth of 25 MHz centered at 2.45 GHz. Hence, the uncoded UCC bit rate is obtained as $(25 \text{ MHz})/(2 \times 256) = 48.8$ kb/s.

Fig. 14 presents a snap-shot of the measured spectrum of the FMT-SS signal at the receiver input along with copies of its zoomed-in versions at two indicated positions in the transmission band. These results are based on samples that were stored while the receiver was operating in real-time. The presence of multipath has led to some frequency selectivity in the channel. Also, the zoomed-in portions clearly resemble the anticipated spectral variation described in Section IV.

Fig. 15 presents a snap-shot of the matched filter output, $z(t)$. We note that, in the presence of the channel, $z(t)$ is a complex-valued baseband signal. Thus, it is presented as a signal with real and imaginary parts. Also, note the presence and absence of the narrow pulses at the points between the successive bits, as one would expect, depends on these bits being similar or different, respectively. Within the present time scale it is hard to see the multipath channel effect. However,

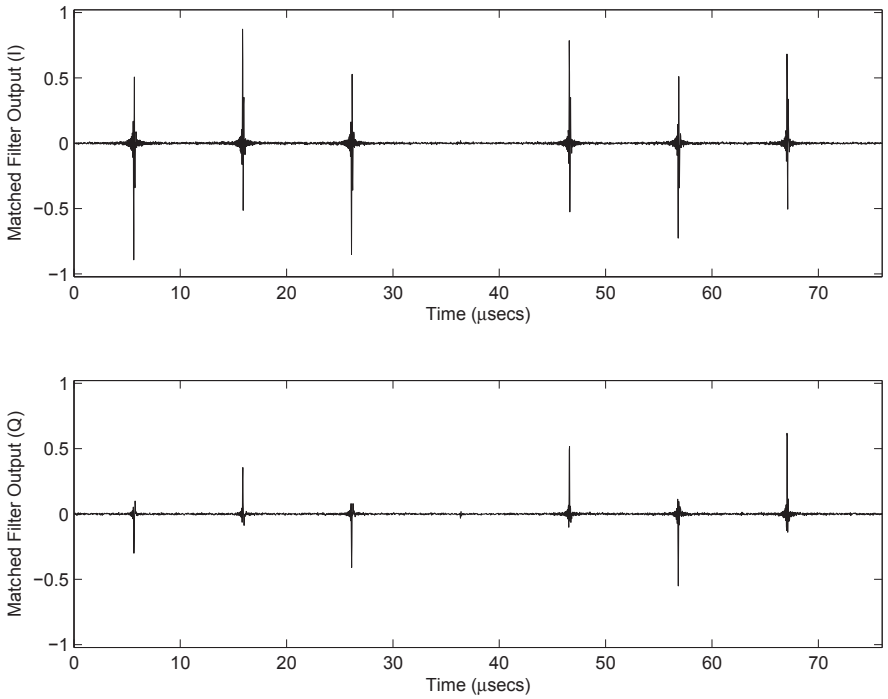

Fig. 15. A captured sample of the matched filter output (high SNR). (a) Real part/in-phase. (b) Imaginary part/quadrature.

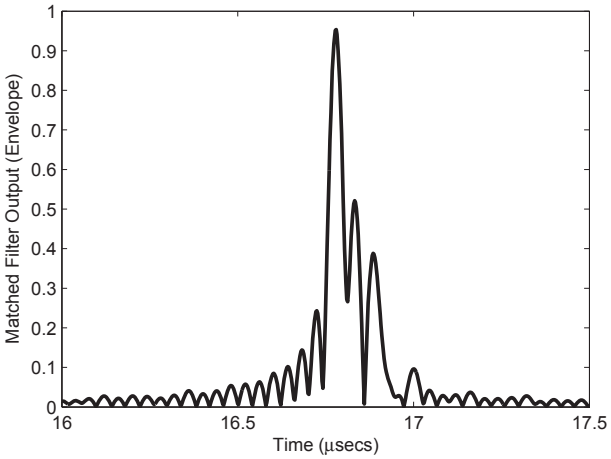

Fig. 16. Magnitude of one pulse at the matched filter output. A number of multipaths are visible around the main peak of the captured pulse.

the multipaths can be seen if we zoom-in on one of the pulses and present its magnitude as a function of time. An example of such presentation is given in Fig. 16. We note that although the multipaths are spread across time at the matched filter output, the MRC combines them in an optimal sense and delivers the estimates of the transmitted bits at a maximum SNR.

Further results are presented in Figs. 17 and 18. The result presented in Fig. 17 is the amplitude of signal output from the matched filter, when the transmitted signal is attenuated to a level where the received signal has an SNR of approximately equal to zero. Note that in this case, also, because of the processing gain of the SS signal the matched filter output has a sufficient amplitude to be distinguishable from the background noise.

Fig. 18 repeats the above experiment under the condition where 50% of the transmission band is occupied by the PUs at a level 20 dB above the SS signal and the cognitive network deactivates the subcarriers that coincide with the active primary bands. The result presented in Fig. 18 confirms that under this condition still UCC remain quite effective. Hence, one may argue that even the presence of significant activity from the PUs does not render the capability of the proposed UCC ineffective. The UCC degrades gradually and may fail only when most of the spectrum is occupied by the PUs. Of course, under such a condition there will not be much spectrum available to the cognitive radios, hence, no significant loss to the cognitive radio network.

VIII. Conclusion

In this paper, we laid out the structure of a filter bank-based multicarrier spread spectrum (FBMC-SS) system as an underlay control channel (UCC) for cognitive radios. The filtered multitone (FMT) was identified as a best choice for the design and implementation of such a UCC. The properties of the proposed FMT-SS system that would allow development of timing and carrier recovery loops were formulated and examples of implementations of the loops on a hardware platform were reported. It was also noted that an optimum receiver requires implementation of a maximum ratio combiner (MRC) that constructs an estimate of each transmit symbol by linearly combining the outputs from an analysis filter bank. Such combiner requires estimates of the channel response at each subcarrier band. We developed a blind channel estimator to take care of this need in the system. Finally, experimental results that highlight the key advantages of the proposed UCC were presented. In particular, it was noted that the presence of the PUs does not render the ability of the UCC to remain

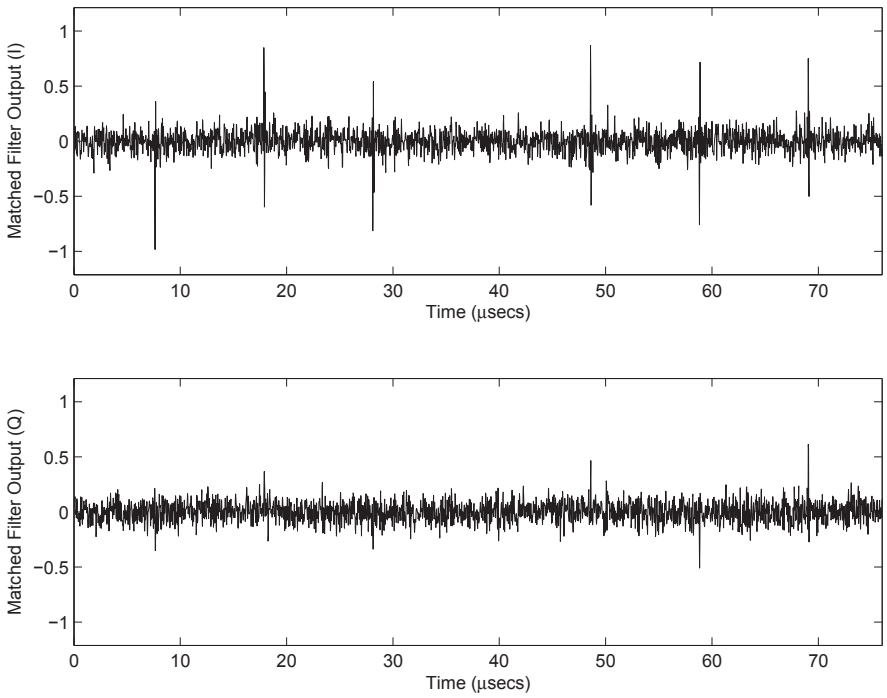

Fig. 17. A captured sample of the matched filter output (low SNR). (a) Real part/in-phase. (b) Imaginary part/quadrature.

effective, unless almost the whole spectrum is occupied by the PUs. Clearly, under this extreme case, the best choice for a cognitive radio network is to shut-down and wait for the next spectrum opportunity.

At the time of writing of this paper, we have been working on the deployment of the proposed UCC in a cognitive radio network consisting of three or more nodes. The result of this study, that will involve development of a medium access control (MAC) layer and some limited upper layers, will be the subject of our future publications.

APPENDIX: PROCESSING GAIN OF FMT-SS

Consider an FMT-SS transceiver systems consisting of the L-fold expander, the transmit filter $g[n]$, an additive white Gaussian noise (AWGN) channel, and a receiver consisting of the matched filter $g^*[-n]$, an L-fold decimator, and a gain of $1/N$, as in Fig. 19. We note that when the channel is AWGN, the receiver in Fig. 19 delivers the same output as the MRC. Hence, the output $\hat{s}[n]$ is that of an optimum detector. We also recall the definition for the processing gain

$$\mathcal{G} = \frac{\rho_{\text{out}}}{\rho_{\text{in}}} \tag{39}$$

where ρ_{in} and ρ_{out} denote SNR at the receiver input and output, respectively.

It also follows from Fig. 19 that

$$\rho_{\text{in}} = \frac{\sigma_x^2}{\sigma_\nu^2} = \frac{N\sigma_s^2}{L\sigma_\nu^2} \tag{40}$$

where σ_x^2 and σ_ν^2 are the variances of $x[n]$ and $\nu[n]$, respectively, and the second line follows since

$$\sigma_x^2 = \sigma_s^2 \times \frac{1}{L} \times \frac{1}{2\pi}\int_0^{2\pi} |G(e^{j\omega})|^2 d\omega,$$

and it follows from (4) that

$$\frac{1}{2\pi}\int_0^{2\pi} |G(e^{j\omega})|^2 d\omega = \frac{N}{2\pi}\int_0^{2\pi} |H(e^{j\omega})|^2 d\omega = N.$$

On the other hand, the detector output $\hat{s}[n]$ may be written as

$$\hat{s}[n] = s[n] + \nu_{\text{out}}[n] \tag{41}$$

where $\nu_{\text{out}}[n]$ is the noise at the detector output. Moreover, it follows from Fig. 19 that

$$\sigma_{\nu_{\text{out}}}^2 = \sigma_\nu^2 \times \frac{1}{2\pi}\int_0^{2\pi} |G^*(e^{j\omega})|^2 d\omega \times \frac{1}{N^2} = \frac{\sigma_\nu^2}{N}. \tag{42}$$

Hence

$$\rho_{\text{out}} = \frac{\sigma_s^2}{\sigma_{\nu_{\text{out}}}^2} = \frac{N\sigma_s^2}{\sigma_\nu^2} \tag{43}$$

Substituting (40) and (43) into (39), we obtain $\mathcal{G} = L$.

The interesting result here is that the processing gain is independent of the number of subcarriers, N. This observation may be counter intuitive. Following the results from DS-SS/CDMA, one may imagine that the processing gain should be equal to the number of spreading gains, which in FMT-SS is equal to the number of subcarriers, N. This peculiar result is related to the magnitude response of the pulse-shaping filter $g[n]$. Recall from Fig. 3(a) that $g[n]$ is a multi-band filter with N subcarrier bands. The receiver matched filter $g^*[-n]$ also has the same magnitude response. When the channel noise passes through this matched filter, its spectrum is shaped and, accordingly, part of its power is removed. The signal part of the received signal, $x[n]$, on the other hand, has a multi-band spectrum that matches the receiver matched filter and thus passes through it without any spectral removal.

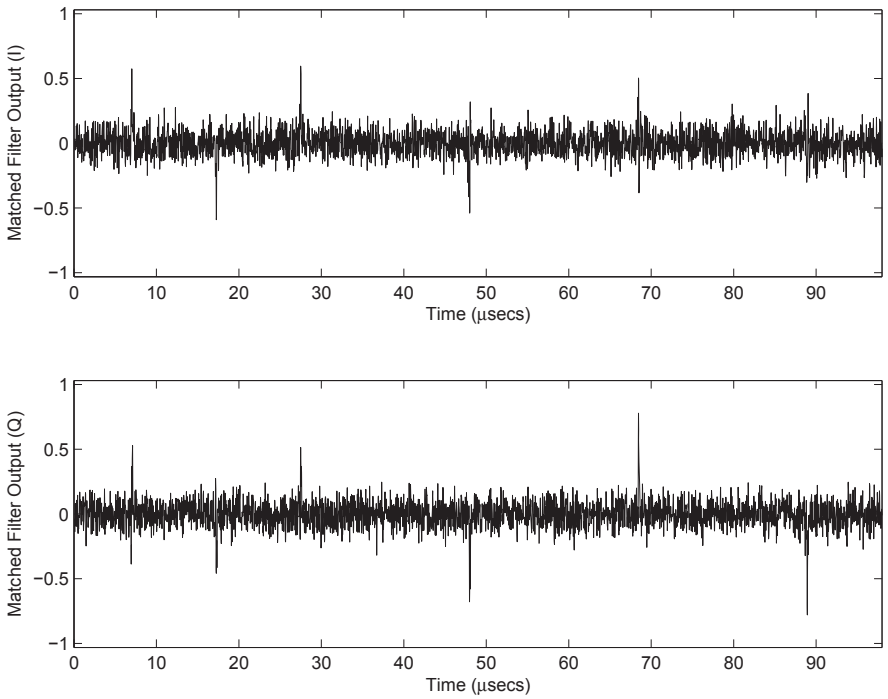

Fig. 18. A captured sample of the matched filter output (low SNR and partial band interference). (a) Real part/in-phase. (b) Imaginary part/quadrature.

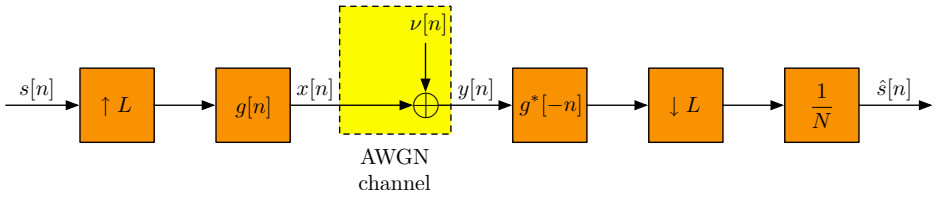

Fig. 19. An FMT-SS transceiver with an AWGN channel.

REFERENCES

[1] Z. Quan, S. Xui, A. Sayed, and H. Poor, "Optimal multiband joint detection for spectrum sensing in cognitive radio networks," *IEEE Trans. Signal Proc.*, vol. 57, no. 3, pp. 1128–1140, March 2009.

[2] B. Farhang-Boroujeny, "Filter bank spectrum sensing for cognitive radios," *IEEE Trans. Signal Proc.*, vol. 56, no. 5, pp. 1801–1811, May 2008.

[3] P. D. Sutton, K. E. Nolan, and L. E. Doyle, "Cyclostationary signatures in practical cognitive radio applications," *IEEE J. Sel. Areas Commun.*, vol. 26, no. 1, pp. 13–24, Jan. 2008.

[4] S. Haykin, "Cognitive radio: Brain-empowered wireless communications," *IEEE J. Sel. Areas Commun.*, vol. 23, no. 2, pp. 201–220, Feb. 2005.

[5] S. Hara and R. Prasad, "Overview of multicarrier CDMA," *IEEE Commun. Mag.*, vol. 35, no. 2, pp. 126–133, Feb. 1997.

[6] S. Kondo and L. B. Milstein, "Performance of multicarrier DS CDMA systems," *IEEE Trans. Commun.*, vol. 44, no. 2, pp. 238–246, Feb. 1996.

[7] G. K. Kaleh, "Overview of multicarrier CDMA," *IEEE Trans. Commun.*, vol. 44, no. 7, pp. 886–893, July 1996.

[8] K. Cheun, K. Choi, H. Lim, and K. Lee, "Anti jamming performance of a multicarrier direct-sequence spread-spectrum system," *IEEE Trans. Commun.*, vol. 47, no. 12, pp. 1781–1784, Dec. 1999.

[9] B. Farhang-Boroujeny and C. Furse, "A robust detector for multicarrier spread spectrum transmission over partially jammed channels," *IEEE Trans. Signal Proc.*, vol. 53, no. 3, pp. 1038–1044, March 2005.

[10] I. F. Akyildiz, W.-Y. Lee, M. C. Vuran, and S. Mohanty, "Next generation/dynamic spectrum access/cognitive radio wireless networks: A survey," *Computer Networks*, vol. 50, no. 13, pp. 2127–2159, Sept. 2006.

[11] I. F. Akyildiz, W.-Y. Lee, and K. R. Chowdhury, "CRAHNs: Cognitive radio ad hoc networks," *Ad Hoc Networks*, vol. 7, no. 5, pp. 810–836, July 2009.

[12] S. M. Mishra, A. Sahai, and R. W. Brodersen, "Cooperative sensing among cognitive radios," *IEEE International Conference on Communications, ICC '06*, vol. 4, pp. 1658–1663, June 2006.

[13] D. Cabric and R. Brodersen, "Physical layer design issues unique to cognitive radio systems," *Personal, Indoor and Mobile Radio Communications*, vol. 2, pp. 759–763, Sept. 2005.

[14] J. Zhao, H. Zheng, and G.-H. Yang, "Distributed coordination in dynamic spectrum allocation networks," *Proc. IEEE DySPAN*, pp. 259–268, Nov. 2005.

[15] L. Cao and H. Zheng, "Distributed spectrum allocation via local bargaining," *in proceedings of Second Annual IEEE Comm. Society Conference on Sensor and Ad Hoc Communications and Networks*, pp. 475–486, Sept. 2005.

[16] K. R. Chowdhury and I. F. Akyildiz, "OFDM-based common control channel design for cognitive radio ad hoc networks," *IEEE Trans. Mobile Computing*, vol. 10, pp. 228–238, 2011.

[17] B. Hamdaoui and K. G. Shin, "OS-MAC: An efficient MAC protocol for spectrum-agile wireless networks," *IEEE Trans. Mobile Computing*, vol. 7, no. 8, pp. 915–930, Aug. 2008.

[18] D. Cabric, S. Mishra, D. Willkomm, R. Brodersen, and A. Wolisz, "A cognitive radio approach for usage of virtual unlicensed spectrum," *in proceedings: 14th IST Mobile and Wireless Communications Summit, Dresden, Germany*, June 2005.

[19] C. Cordeiro and K. Challapali, "C-MAC: A cognitive MAC protocol for multi-channel wireless networks," *in Proc. IEEE Int. Symp. on Dynamic Spectrum Access (DySPAN)*, pp. 147–157, Apr. 2007.

[20] J. Jia, Q. Zhang, and X. Shen, "HC-MAC: a hardware constrained cognitive MAC for efficient spectrum management," *IEEE J. Sel. Areas Commun.*, vol. 26, no. 1, pp. 106–117, 2008.

[21] C. Cormio and K. R. Chowdhury, "A survey on MAC protocols in

cognitive radio wireless networks," *Ad Hoc Networks*, vol. 7, no. 7, pp. 1315–1329, Sept. 2009.
[22] B. F. Lo, "A survey of common control channel design in cognitive radio networks," *Physical Communication*, vol. 4, pp. 26–39, 2011.
[23] D. Cabric, S. Mishra, and R. Brodersen, "Implementation issues in spectrum sensing for cognitive radios," *IEEE J. Sel. Areas Commun.*, vol. 1, no. 11, pp. 772–776, Nov. 2004.
[24] R.-R. Chen, K.-H. Teo, and B. Farhang-Boroujeny, "Random access protocols for collaborative spectrum sensing in multi-band cognitive radio networks," *IEEE J. Sel. Topics Signal Process.*, vol. 5, no. 2, pp. 124–136, Feb. 2011.
[25] T. Chen, H. Zhang, G. M. Maggio, and I. Chlamtac, "Cogmesh: A cluster-based cognitive radio network," *Proc. IEEE DySPAN*, p. 168178, Apr. 2007.
[26] B. F. Lo, I. F. Akyildiz, and A. M. Al-Dhelaan, "Efficient recovery control channel design in cognitive radio ad hoc networks," *IEEE Trans. Veh. Technol.*, vol. 59, no. 9, pp. 4513–4526, Nov. 2010.
[27] L. A. DaSilva and I. Guerriero, "Sequence-based rendezvous for dynamic spectrum access," *in Proc. IEEE Int. Symp. on Dynamic Spectrum Access (DySPAN)*, pp. 1–7, October 2008.
[28] C. Cormio and K. R. Chowdhury, "Common control channel design for cognitive radio wireless ad hoc networks using adaptive frequency hopping," *Ad Hoc Networks*, vol. 8, pp. 430–438, 2010.
[29] M. E. Sahin and H. Arslan, "System design for cognitive radio communications," *Proc. IEEE CrownCom*, pp. 1–5, June 2006.
[30] M. Petracca, R. F. Pomposini, R. G. Mazzenga, and M. Vari, "An always available control channel for cooperative sensing in cognitive radio networks," *Wireless Days (WD)*, vol. IFIP, p. 15, 2010.
[31] K. Bian, J.-M. Park, and R. Chen, "A quorum-based framework for establishing control channels in dynamic spectrum access networks," *in Proc. MobiCom*, pp. 25–36, 2009.
[32] N. C. Theis, R. W. Thomas, and L. A. DaSilva, "Rendezvous for cognitive radios," *IEEE Trans. Mobile Computing*, vol. 10, pp. 216–227, 2011.
[33] A. Masri, C.-F. Chiasserini, C. Casetti, and A. Perotti, "Common control channel allocation in cognitive radio networks through UWB multihop communications," *in: The First Nordic Workshop on Cross Layer Optimization in Wireless Networks at Levi, Finland*, 2010.
[34] T. Weiss and F. J. et al., "Spectrum pooling: An innovative strategy for the enhancement of spectrum efficiency," *IEEE Commun. Mag.*, vol. 42, no. 3, pp. 8–14, 2004.
[35] B. Farhang-Boroujeny, "OFDM versus filter bank multicarrier," *IEEE Signal Processing Mag.*, vol. 28, no. 3, pp. 92–112, May 2011.
[36] B. Farhang-Boroujeny and R. Kempter, "Multicarrier communication techniques for spectrum sensing and communication in cognitive radios," *IEEE Commun. Mag.*, vol. 46, no. 4, pp. 80–85, April 2008.
[37] P. P. Vaidyanathan, *Multirate Systems and Filter Banks*. Englewood Cliffs, NJ: Prentice-Hall, 1993.
[38] B. Farhang-Boroujeny and C. G. Yuen, "Cosine modulated and offset QAM filter bank multicarrier techniques: A continuous-time prospect," *Eurasip Journal on Advances in Signal processing*, vol. 2010, 2010.
[39] D. Chu, "Polyphase codes with good periodic correlation properties," *IEEE Trans. Inf. Theory*, vol. 18, no. 4, pp. 531–532, Jul. 1972.
[40] B. Farhang-Boroujeny, *Signal Processing Techniques for Software Radios*. Lulu, 2nd edition, 2010.
[41] J. Proakis, *Digital Communications*, 3rd ed. McGraw-Hill, New York, NY, 1995.

Daryl Leon Wasden Daryl Wasden received the B.S. in Electrical Engineering from the University of Utah in 2009 and is poised to receive the M.S. in Electrical and Computer Engineering from the University of Utah in 2012. He is currently working toward his Ph.D. in Electrical and Computer Engineering under the supervision of Dr. Behrouz Farhang-Boroujeny at the University of Utah. He is a recipient of a National Science Foundation (NSF) Graduate Research Fellowship. His research interests include software-defined radio implementation, cognitive radio, filter bank multicarrier communications, spread spectrum communications, and multiple-input multiple-output (MIMO) detection.

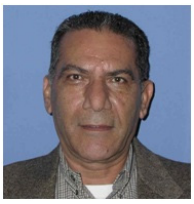

Hussein Moradi Dr. Hussein Moradi brings to Idaho National Laboratory (INL) more than 30 years of experience in various elements of corporate research and development leadership. Dr. Moradi earned his Ph.D. and Masters Degree from Southern Methodist University (SMU), Dallas and his Bachelor Degree from University of Texas at Arlington (UTA); all of the degrees are in the Electrical Engineering discipline. He has been a member of the Board of Professional Engineers w since the early 1990s. Prior to joining INL, Dr. Moradi assumed lead R&D responsibly at NEC America, VeriFone and Kyocera.

Dr. Moradi possesses extensive industry R&D experience developing leading-edge technologies from early incubation to mass production stage. Dr. Moradi's expertise encompasses systems engineering, RF layer, ASIC, hardware and embedded software development for computing and wireless telecommunications devices. In particular, Dr. Moradi has developed GSM/GPRS/EDGE, CDMA/EVDO, 802.11, BT 2.5G/3G VoIP capable wireless handsets and has domain expertise in WiMAX, LTE and future wireless technology trends in physical layer spectrum agile communications.

Behrouz Farhang-Boroujeny Behrouz Farhang-Boroujeny (M'84-SM'90) received the B.Sc. degree in electrical engineering from Teheran University, Iran, in 1976, the M.Eng. degree from University of Wales Institute of Science and Technology, UK, in 1977, and the Ph.D. degree from Imperial College, University of London, UK, in 1981.

From 1981 to 1989 he was with the Isfahan University of Technology, Isfahan, Iran. From 1989 to 2000 he was with the National University of Singapore. Since August 2000, he has been with the University of Utah.

He is an expert in the general area of signal processing. His current scientific interests are adaptive filters, multicarrier communications, detection techniques for space-time coded systems, and cognitive radio. In the past, he has worked and has made significant contribution to areas of adaptive filters theory, acoustic echo cancellation, magnetic/optical recoding, and digital subscriber line technologies. He is the author of the books "Adaptive Filters: theory and applications", John Wiley & Sons, 1998, and Signal Processing Techniques for Software Radios, self published at Lulu publishing house, 2009 and 2010 (second edition).

Dr. Farhang-Boroujeny received the UNESCO Regional Office of Science and Technology for South and Central Asia Young Scientists Award in 1987. He served as an associate editor of IEEE Trans. on Signal Processing from July 2002 to July 2005, and as an associate editor of IEEE Signal Processing Letters from April 2008 to March 2010. He has also been involved in various IEEE activities, including the chairmanship of the Signal Processing/Communications chapter of IEEE of Utah in 2004 and 2005.